

Ripple Effects on Small Signal Models in Average Current Mode Control

Chunxiao Sun[†] Brad Lehman^{†‡} Jian Sun[‡]

[†]IPD/NU DC/DC Converter Research Center, International Power Devices, Inc., 20 Linden St, Boston, MA 02134

[‡]Dept. of Electrical & Computer Engineering, Northeastern University, Boston, MA 02115

[‡]Rockwell Collins, 400 Collins Road NE, Cedar Rapids, IA 52498-3161

ABSTRACT-The effects of switching frequency ripple on the behavior of average current mode PWM DC/DC converters are studied. Ripple estimation and superposition methods are applied to derive new frequency-dependent averaged models that take into account these effects. Small-signal analysis of the new model reveals several important characteristics of average current mode control, especially under large ripple conditions, that previous models are unable to predict. Discussions on the small-signal models for PWM DC/DC converters are demonstrated

I. INTRODUCTION

Average current mode control (ACMC)[1] has several advantages over peak current mode control including 1) elimination of the external compensation ramp to stabilize the current loop, 2) increased DC and low frequency current loop gain because of the use of integrator in the current loop, and 3) improved noise immunity due to the low-pass prediction. Recently, the ripple component of the controller was found to have important effects on both the DC gain and high-frequency phase shift of the current loop [2]. Previous averaged models using conventional averaging techniques were shown to be either unable to predict these ripple effects or become complicated when they are considered.

This paper presents a systematic modeling method for average current mode control that takes into account ripple effects. This method attempts to determine the real duty ratio (termed switching time in this paper) of the average current mode converter. It decomposes output and state variables of the power stage into averaged values plus ripples and then applies superposition on the control loop to estimate the compensator output ripple. This paper will emphasize small-signal analysis of average current mode PWM converters

Almost all-previous work on the modeling of average current mode control is based on conventional averaging techniques that ignore switching ripples [1, 2]. The resulting models work well when the current compensator output has low ripple. However, as has been demonstrated in [2], there are discrepancies between averaged models and measured current loop gain and phase. As this paper shows, for other small signal characteristics such as output impedance, the conventional models may differ drastically than actual values. New, more accurate models are proposed to account for these discrepancies. The results of this work generalize small signal modeling methods of [3,4], which were applied to the specific class of ACMC of buck converters.

In Section II, sample simulation and experimental results are presented that demonstrate inaccuracies in conventional modeling methods. The new modeling method using superposition method is shown to more accurately reflect experiments. Section III resolves conventional small signal inaccuracies by introducing revised small signal models. Section IV gives brief technical details to the derivation of the new models. Section V shows simulation and experimental results of an ACMC boost converter. Section VI presents conclusions.

II. SAMPLE EXAMPLES

A. Incorrect Duty Ratio Prediction

Fig. 1 shows a typical ACMC boost converter. In this topology, there is an inner current loop, $K_i(s)$, that senses the inductor current and uses the output of the outer voltage control loop, $K_v(s)$ as the reference. The output of the inner loop is then compared to an externally provided ramp to generate PWM waveform.

In average current mode control, there is large flexibility in selecting the control schemes for both the inner current

[†] Brad Lehman gratefully acknowledges the support of International Power Devices, and NSF Grant CMS9596268.

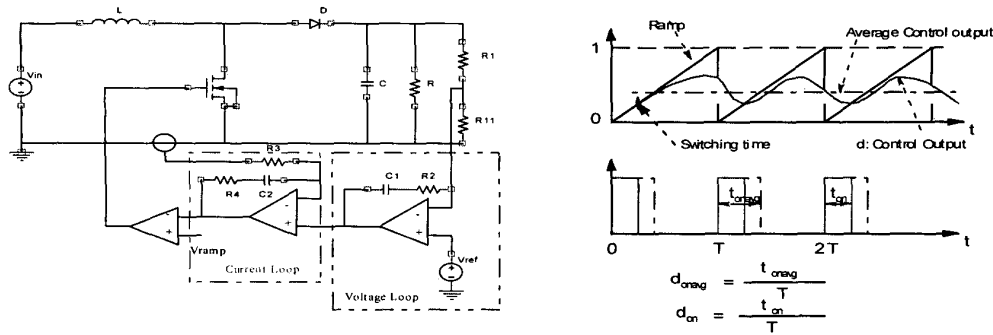


Fig. 1 A Typical Average Current Mode Controlled Boost Converter

loop and the outer voltage loop. The difficulty of modeling the average current mode control lies in the fact that the control output of the DC/DC converter may have large, non-triangular ripple as shown in Fig. 1. The duty ratio generated by average control output (d_{avg}) is no longer equal to the real duty ratio. Here in this paper, we term the real duty ratio switching time $\tau_i \equiv d_{on}$, since the switching behavior takes place at that instant. The relationship between switching time and averaged control output is described by a nonlinear equation as will be shown in Section IV.

B. Small Signal Experiments: Output Impedance

Input and output impedance are the basis for stability analysis of systems involving switching power converters. Such a system may be as simple as a single converter with an input EMI filter, or as a large distributed power system that uses tens or even hundreds of converters. Accurate prediction of impedance characteristics for each converter is essential for correct assessment of system stability and design optimization [9,11]. Fig. 2 shows the output impedance of an ACMC boost converter with two PI controllers for both inner current and outer voltage loop. In Fig. 2, we can see that output impedance predicted by new, superposition models match the measurement result well, while large magnitude and phase discrepancies are detected between conventional models and measurement.

The errors in conventional models are drastic and could lead to instabilities. Typical impedance matching stability criteria [11] requires that $|Z_o| < |Z_i|$, where Z_i is the input impedance of the load subsystem. Notice that conventional models predict that $|Z_o|_{max} \approx 0dB$, when in fact, it has been measured to be approximately 20 dB. The new models predict $|Z_o|_{max} \approx 18dB$, which is a clear improvement.

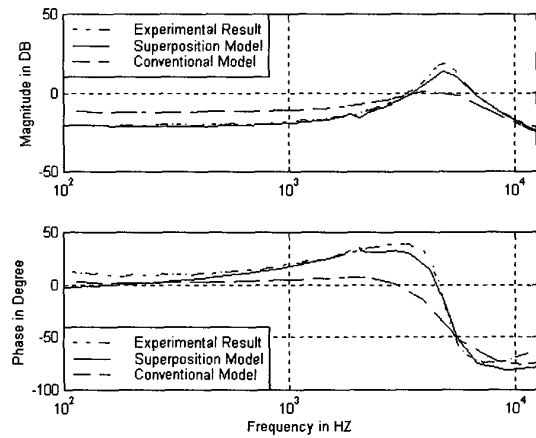


Fig. 2 Output Impedance of Average Current Mode Boost Converter ($f_s = 25kHz$, $V_m = 10.0V$, $L = 70\mu H$, $C = 21\mu F$, $R = 10.3\Omega$, $K_i(s) = 4.84 + 100.3/s$, $K_v(s) = 0.01 + 10.4/s$, $D = 0.31$, $K_s = 0.2$)

III. Small Signal Models

Figure 3 illustrates the newly proposed block diagram representation of small signal transfer functions for ACDC PWM DC/DC converters. In this figure M_1 , M_2 , M_3 represent the open loop audio susceptibility, control to output transfer function and output impedance respectively; N_1 , N_2 , N_3 represents the open loop input admittance, control to inductor current transfer function, and current sensitivity respectively. $K_i(s)$ and $K_v(s)$ are current loop and voltage loop controllers, and K_s represents current sensing gain.

The structure of Fig. 3 is similar to that proposed in [4] for peak current mode control, with the important exception that the influence of transfer functions $\Delta(s, T)$, $H_i(s, T)$ and $H_v(s, T)$ have been included to provide gain adjustment and phase shift due to ripples. In fact, in [3, 4],

TABLE 1. LOOP GAINS AND CLOSED LOOP TRANSFER FUNCTIONS

Transfer functions	Conventional Models	Superposition Models
Current Loop Gain	$T_i = K_i K_r N_i$	$\tilde{T}_i = T_i / \Delta$
Voltage Loop Gain	$T_v = K_v (1 + K_r) M_i$	$\tilde{T}_v = T_v / \Delta$
Total Loop Gain	$T_i + T_v$	$\tilde{T}_i + \tilde{T}_v$
Audio Susceptibility	$\frac{M_i (1 + T_i) - \frac{M_i T_i N_i}{N_i}}{1 + T_i + T_v}$	$\frac{M_i (1 + \tilde{T}_i) - \frac{M_i \tilde{T}_i}{N_i} N_i + \frac{M_i H_r}{\Delta}}{1 + \tilde{T}_i + \tilde{T}_v}$
Output Impedance	$\frac{M_i (1 + T_i) - \frac{M_i T_i N_i}{N_i}}{1 + T_i + T_v}$	$\frac{M_i (1 + \tilde{T}_i) - \frac{M_i \tilde{T}_i}{N_i} N_i + \frac{M_i H_i}{\Delta}}{1 + \tilde{T}_i + \tilde{T}_v}$
Input Admittance	$\frac{N_i (1 + T_v) - \frac{M_i N_i T_v}{M_i}}{1 + T_i + T_v}$	$\frac{N_i (1 + \tilde{T}_v) - \frac{N_i \tilde{T}_v}{M_i} M_i + \frac{N_i H_v}{\Delta}}{1 + \tilde{T}_i + \tilde{T}_v}$
Current Sensitivity	$\frac{N_i (1 + T_v) - \frac{M_i N_i T_v}{M_i}}{1 + T_i + T_v}$	$\frac{N_i (1 + \tilde{T}_v) - \frac{N_i \tilde{T}_v}{M_i} M_i + \frac{N_i H_i}{\Delta}}{1 + \tilde{T}_i + \tilde{T}_v}$

$$\Psi_d = C_c \int_0^{A_c(t-\tau)} B_c [\Psi_{v_o}(\tau) \quad \Psi_{v_i}(\tau)]^T d\tau + K_c [\Psi_{v_o}(\tau) \quad \Psi_{v_i}(\tau)]^T \quad (2)$$

Here $\Psi_{v_i} = K_i \Psi_i$, where K_i is the current sensing gain.

The reader is referred to [7] and the Appendix to view the specific details of the solution of this equation.

In essence, the proposed method performs averaging for the important dynamics below one third of the switching frequency and explicitly solves for the important faster dynamics that contribute to system behavior. Once Ψ_d is solved for, we find the switching time τ_s by solving the nonlinear algebraic equation (1). It is important to note that the ripple Ψ_d is dependent on many variables, i.e., $\Psi_d = \Psi_d(t, V_m, T, \langle i_l \rangle, \langle v_o \rangle, \tau_s)$. In order to obtain small signal transfer functions, we linearize (1) with $t = \tau_s T$ to obtain

$$\tilde{d} + \frac{\partial \Psi_d}{\partial \tau_s} \tilde{\tau}_s + \frac{\partial \Psi_d}{\partial V_m} \tilde{V}_m + \frac{\partial \Psi_d}{\partial i_l} \tilde{i}_l + \frac{\partial \Psi_d}{\partial v_o} \tilde{V}_o = \tilde{\tau}_s V_p \quad (3)$$

Open loop small signal transfer functions give

$$\tilde{i}_l = N_1 \tilde{V}_m + N_2 \tilde{\tau}_s + N_3 \tilde{i}_o \quad (4)$$

and

$$\tilde{v}_o = M_1 \tilde{V}_m + M_2 \tilde{\tau}_s + M_3 \tilde{i}_o \quad (5)$$

Taking Laplace transform, and substituting (4) and (5) into (3), we see that

$$\tilde{\tau}_s(s) = \frac{H_v(s, T) \tilde{V}_m(s) + H_i(s, T) \tilde{i}_o(s) + \tilde{d}(s)}{\Delta(s, T)} \quad (6)$$

Where

$$H_v(s, T) = \partial \Psi_d / \partial V_m + N_1 \partial \Psi_d / \partial i_l + M_1 \partial \Psi_d / \partial v_o \quad (7)$$

$$H_i(s, T) = \partial \Psi_d / \partial i_o + N_2 \partial \Psi_d / \partial i_l + M_2 \partial \Psi_d / \partial v_o \quad (8)$$

$$\Delta(s, T) = V_p - \partial \Psi_d / \partial \tau_s - N_3 \partial \Psi_d / \partial i_l - M_3 \partial \Psi_d / \partial v_o \quad (9)$$

Hence, the small signal models of Section III and Fig. 6 are now directly derived. Notice that the steady state values are used in calculating these partial derivatives such as $\partial \Psi_d / \partial \tau_s$, $\partial \Psi_d / \partial i_l$, $\partial \Psi_d / \partial v_o$ and $\partial \Psi_d / \partial i_o$, e.g. $\partial \Psi_d / \partial i_o = \partial \Psi_d / \partial i_o \big|_{\langle i_l \rangle = \tilde{i}_l, \langle v_o \rangle = \tilde{v}_o, \langle v_m \rangle = V_m}$ or we can see that these are constant coefficients. Again it is important for us to notice that $1/\Delta(s, T)$ is actually the modulator gain looked for by [3] and [4].

V. Small Signal Simulation and Experiments

Simulation and experimentation is performed on a ACDC boost converter shown in Fig.1 with PI controllers for both current loop and voltage loop. The parameters used in the simulation and experimentation are as following: $V_{in} = 10.0V$, $L = 172\mu H$, $C = 21\mu H$, $R = 10.3\Omega$. The output

voltage is 12.6 V. The switching frequency is 25kHz. The current sensing gain is $K_s = 0.2$. The controllers are chosen as $K_i(s) = 2.42 + 22E3/s$ for current loop and $K_v(s) = 0.1 + 11.46/s$ for voltage loop for simulation. The results obtained in Fig.6 apply $K_v(s) = 0.05 + 11.46/s$ for voltage loop.

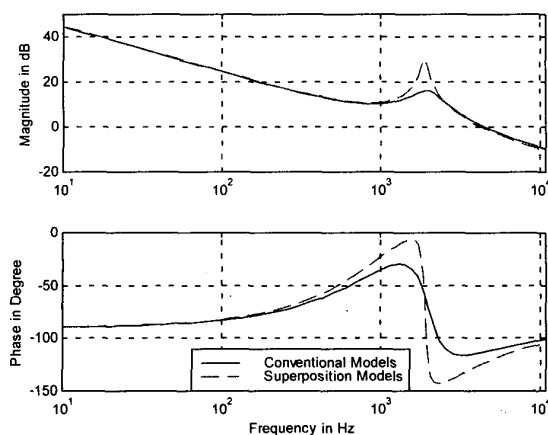


Fig. 4 Current Loop gain

In Fig. 4, the phase margin estimated by conventional models is 66.78 degree at 4.4kHz, different from that of the superposition models giving 55 degree of phase margin at 4.2kHz. Larger phase and magnitude discrepancy may occur using other control parameters. It is always possible that conventional models always predict phase margin in the desired range ($\geq 45^\circ$), while the real phase margin falls below the desired range. This is also true for voltage loop gain and total loop gain.

Magnitude and phase discrepancy also occur in close loop performance transfer functions such as output impedance, input admittance and current sensitivity. Fig. 5 shows the simulation results of the input impedance. Large magnitude and phase discrepancy occur around resonant frequency between these two models.

Fig. 6 shows the lab measurement for inner loop gain $\tilde{T}_i / (1 + \tilde{T}_v)$ derived by breaking the loop at negative input of the current loop controller. It can be seen that the prediction by conventional models give up to 5dB difference in magnitude with that of the lab measurement, while only 0.5dB difference is observed by superposition models.

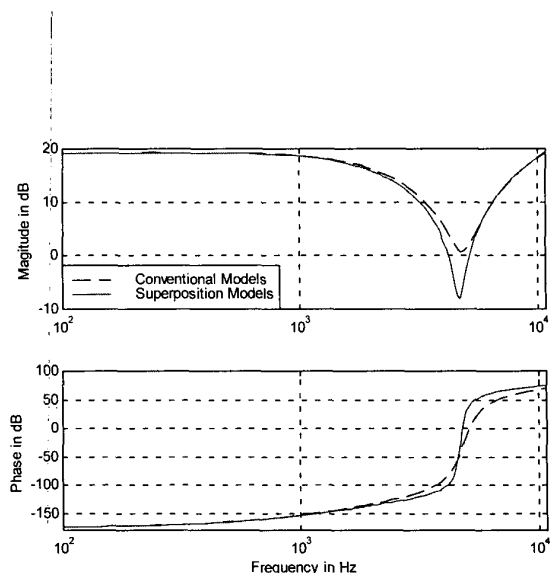


Fig.5 Input Impedance

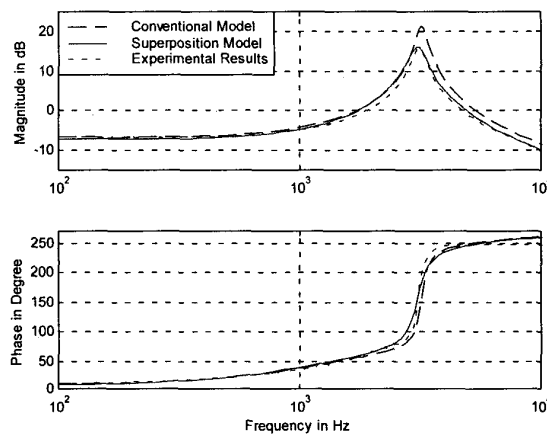


Fig. 6 Lab Measurement for Inner Loop Gain

VI CONCLUSIONS

Average current mode is known for its tendency of having large ripple on control loop. The ripple effect the frequency domain response has been observed, which can not be predicted by conventional models. Superposition models are verified to be more accurate than conventional models in small signal prediction. Both theoretical justification and experimental results are provided to demonstrate the ripple effect of average current mode control. Overall, method proposed in this paper for the derivation of small signal models provides a general approach to accurately predict behaviors of average current mode PWM DC/DC converters.

REFERENCES

- [1] L. H. Dixon, "Average Current Mode Control of Switching Power Supplies," Unitrode Power Supply Design Seminar Manual, 1990.
- [2] J. Sun and R. M. Bass, "Modeling and Practical Design Issues for Average Current Control", *Applied Power Electronics Conference*, 1999
- [3] W. Tang, F. C. Lee, and R. B. Ridley, "Small Signal Modeling of Average Current Mode Control," *IEEE Transactions on Power Electronics*, Vol. 8, No. 2, pp.112-119, 1993.
- [4] Yen-Wu Lo and R. J. King, "Sampled-Data Modeling of Average-Input Current-Mode-Controlled Buck Converter," *IEEE Transactions on Power Electronics*, VOL. 14, NO. 5, pp. 918-927, Sept. 1999.
- [5] R. B. Ridley, "Analysis and Interpretation of Loop Gains of Multiloop-Controlled Switching regulators," *IEEE Transactions on Power Electronics*, Vol. 3, No. 4, pp. 489-498, 1988.
- [6] B. Lehman and R. M. Bass, "Switching Frequency Dependent Averaged Models for PWM DC-DC converters," *IEEE Transactions on Power Electronics*, Vol.11, pp. 542-553, Jul., 1996.
- [7] C. Sun, B. Lehman and R. Ciprian, "Dynamic Modeling and Control in Average Current Mode Controlled PWM DC/DC converters," in *IEEE PESC'99 Records*, pp.1152-1158.
- [8] B. Lehman and Z. Mihajlovic, "Output Ripple Analysis of Switching DC-DC Converters," in *IEEE PESC'97 Records*, pp775-781.
- [9] R. D. Middlebrook, "Measurement of loop Gain in feedback Systems", *Int. J. Electronics*, 1975, vol. 38, pp. 485-512.
- [10] R. M. Bass and J. Sun, "Large Signal Averaging Method under Large Ripple Conditions," in *IEEE PESC'98 Records*, pp. 615-622.
- [11] X. Feng, Z. Ye, K. Xing, F. C. Lee and D. Borojevic, "Impedance Specification and Impedance improvement for DC Distributed Power System," in *IEEE PESC'99 Records*, pp.889-894.

APPENDIX: Derivation of Ripple on Control Output at Switching Time for APMC Boost Converter with PI Controllers

Generally, power stage switching models for an APMC DC/DC converter operating in continuous conduction mode can be written as [6]:

$$\begin{aligned} \dot{x} &= A_s x + B_s V_u + E_s i_s + G_s + (A_s x + B_s V_u + E_s i_s + G_s)h(d - \text{tri}(t, T)) \\ y &= C_s x + H_s i_s + F_s + (C_s x + H_s i_s + F_s)h(d - \text{tri}(t, T)) \end{aligned} \quad (\text{A.1})$$

where h is the heavy-side function taking value 1 when the control output d is greater than the ramp represented by $\text{tri}(t, T)$, and 0 vice versus. The control circuitry can be represented by linear differential equations with periodic inputs: output voltage v_c and inductor current i_c , shown in (A.2),

$$\begin{aligned} \dot{x}_c &= A_c x_c + B_c U + G_c V_u \\ d &= C_c x_c + K_c U + E_c V_u \end{aligned} \quad (\text{A.2})$$

For a boost converter shown in Fig. 1 with parasitic considered above, we have the matrices:

$$\begin{aligned} A_n &= \begin{bmatrix} -\frac{\alpha R_c + R_L + R_o}{L} & -\frac{\alpha}{L} \\ \frac{\alpha}{C} & -\frac{1}{L(R+R_c)} \end{bmatrix}, & A_i &= \begin{bmatrix} R_o - R_o + \alpha R_c & \alpha \\ \frac{L}{C} & 0 \end{bmatrix}, \\ B_n &= \begin{bmatrix} \frac{1}{L} \\ 0 \end{bmatrix}, & B_i &= 0, & E_n &= \begin{bmatrix} -\alpha R_c \\ \alpha \end{bmatrix}, & E_i &= \begin{bmatrix} \alpha R_c \\ -2\alpha \end{bmatrix}, \\ C_n &= [\alpha R_c \quad \alpha], & C_i &= [-\alpha R_c \quad 0], & H_n &= \alpha R_c, & H_i &= -2\alpha R_c, \\ G_n &= \begin{bmatrix} -\frac{V_o}{L} \\ 0 \end{bmatrix}, & G_i &= \begin{bmatrix} \frac{V_o}{L} \\ 0 \end{bmatrix} & \text{and } F_n &= F_i = 0 \text{ for power stage in} \end{aligned}$$

(A.1), where $x = [i_c \quad v_c]^T$ and $y = v_c$. A typical two-loop PI control circuitry takes form of $K_c(s) = K_n + \frac{K_p}{s}$ for current loop and

$K_v(s) = K_n + \frac{K_p}{s}$ for voltage loop. The state space expression is given by (A.2) with $A_c = \begin{bmatrix} 0 & 0 \\ K_n & 0 \end{bmatrix}$, $B_c = \begin{bmatrix} 0 & K_n \\ K_n K_i & K_n K_v \end{bmatrix}$, $G_c = \begin{bmatrix} -K_n \gamma \\ -K_n K_n \gamma \end{bmatrix}$, $C_c = [-(1+K_n) \quad -1]$, $K_c = [-(1+K_n)K_n \quad -K_n K_i]$, $E_c = K_n(1+K_n)\gamma$. where γ is used to balance the reference voltage in voltage loop.

The ripple on the power stage state variables are obtained by using the formula in [6]:

$$\begin{aligned} \Psi_{i_c}(t) &= \begin{bmatrix} m_1(t - \frac{\tau_s T}{2}), & 0 \leq t \leq \tau_s T \\ m_2(t - \frac{(1+\tau_s)T}{2}), & \tau_s T \leq t \leq T \end{bmatrix} \\ &(\text{A.3}) \\ \Psi_{v_c}(t) &= \begin{bmatrix} n_1(t - \frac{\tau_s T}{2}), & 0 \leq t \leq \tau_s T \\ n_2(t - \frac{(1+\tau_s)T}{2}), & \tau_s T \leq t \leq T \end{bmatrix} \end{aligned} \quad (\text{A.4})$$

where

$$m_1 = (\frac{R_o - R_o + \alpha R_c}{L} <i_c> + \frac{\alpha}{L} <v_c>)(1-\tau_s), \quad m_2 = -m_1 \tau_s / (1-\tau_s),$$

$$n_1 = -\frac{\alpha}{C} <i_c> (1-\tau_s) \text{ and } n_2 = -n_1 \tau_s / (1-\tau_s).$$

The ripple on the output of power stage is given as [8]

$$\Psi_{v_c}(t) = \begin{bmatrix} \alpha \Psi_{i_c} - \alpha R_c (1-\tau_s) <i_c>, & 0 \leq t \leq \tau_s T \\ \alpha R_c \Psi_{i_c} + \alpha \Psi_{v_c} + \alpha R_c \tau_s <i_c>, & \tau_s T \leq t \leq T \end{bmatrix} \quad (\text{A.5})$$

Substituting (A.3), (A.4) and (A.5) into (2), we have the following equation giving the value of the control output at switching time.

$$\begin{aligned} \Psi_{i_c}(\tau_s T) &= J_{z1} <i_c> \tau_s + J_{z2} <i_c> \tau_s + (J_{z3} <i_c> + J_{z4} <v_c>) \tau_s + \\ &(J_{z5} <i_c> - J_{z6} <v_c>) \tau_s + J_{z6} <i_c> \end{aligned} \quad (\text{A.6})$$

where

$$\begin{aligned} J_{z1} &= \frac{K_n K_n \alpha^2 T^2}{12C}, & J_{z2} &= -J_{z1} + \frac{K_n k_c \alpha R_c T}{2L} - \frac{K_n K_n \alpha R_c T^2}{2}, \\ J_{z3} &= -(J_{z1} + J_{z2}) - ((1+K_n)K_n + K_n K_n) \alpha R_c T - \frac{(1+K_n)K_n \alpha^2 T}{2C} \\ J_{z4} &= -(J_{z1} + J_{z2} + J_{z3}) - (1+K_n)K_n \alpha R_c, & J_{z5} &= -(J_{z1} + J_{z2} + J_{z3} + J_{z4}), \\ J_{z6} &= -J_{z1} = -\frac{K_n k_c T}{2L} \end{aligned}$$

It can be seen from (A.6) that the control output ripple at the switching time is the function of switching time, power stage averaged state variable $<i_c>$ and output voltage $<v_c>$. Since averaged variables finally will be described in term of input voltage V_u , load current i_c and switching time τ_s , the output ripple at switching time as given in (A.6) is actually a function of V_u , i_c and τ_s . Therefore, it is plausible to write the control output ripple at switching time in either of these two forms: $\Psi_{i_c}(\tau_s T, <i_c>, <v_c>)$ and $\Psi_{i_c}(\tau_s T, i_c, V_u)$. This recognition has been very helpful in deriving small signal models.